Title
Semi-automated protocol to quantify and characterize fluorescent three-dimensional vascular images

Journal
PLOS ONE, 19(5)

ISSN
1932-6203

Authors
Xie, Danny F
Crouzet, Christian
LoPresti, Krystal
et al.

Publication Date
2024

DOI
10.1371/journal.pone.0289109

PLOS ONE

LAB PROTOCOL

Semi-automated protocol to quantify and characterize fluorescent three-dimensional vascular images

Danny F. Xie[1,2], Christian Crouzet[1,2], Krystal LoPresti[1,2], Yuke Wang[1,2], Christopher Robinson[1,2], William Jones[1], Fjolla Muqolli[1], Chuo Fang[3], David H. Cribbs[4], Mark Fisher[1,3,4,5], Bernard Choi[1,2]*

1 Beckman Laser Institute and Medical Clinic, University of California-Irvine, Irvine, CA, United States of America, **2** Department of Biomedical Engineering, University of California-Irvine, Irvine, CA, United States of America, **3** Department of Neurology, University of California-Irvine, Irvine, CA, United States of America, **4** Institute for Memory Impairments and Neurological Disorders, University of California-Irvine, Irvine, CA, United States of America, **5** Department of Pathology & Laboratory Medicine, University of California-Irvine, Irvine, CA, United States of America

* choib@uci.edu

OPEN ACCESS

Citation: Xie DF, Crouzet C, LoPresti K, Wang Y, Robinson C, Jones W, et al. (2024) Semi-automated protocol to quantify and characterize fluorescent three-dimensional vascular images. PLoS ONE 19(5): e0289109. https://doi.org/10.1371/journal.pone.0289109

Editor: David Mayerich, University of Houston, UNITED STATES

Received: August 30, 2022

Accepted: July 11, 2023

Published: May 16, 2024

Data Availability Statement: All relevant data are available from Figshare (https://doi.org/10.6084/m9.figshare.20330475.v1).

Funding: This work was supported in part by the National Institutes of Health (R21AG066000 to DX and BC, 5TL1TR001415-07 to CC, R21NS111984 to DC, MF, and BC, R01NS020989 to DC, MF, and BC, P41EB015890 to BC, http://www.nih.gov/) and the Arnold and Mabel Beckman Foundation (http://www.beckman-foundation.org/) to BC. The funders had no role in study design, data collection and

Abstract

The microvasculature facilitates gas exchange, provides nutrients to cells, and regulates blood flow in response to stimuli. Vascular abnormalities are an indicator of pathology for various conditions, such as compromised vessel integrity in small vessel disease and angiogenesis in tumors. Traditional immunohistochemistry enables the visualization of tissue cross-sections containing exogenously labeled vasculature. Although this approach can be utilized to quantify vascular changes within small fields of view, it is not a practical way to study the vasculature on the scale of whole organs. Three-dimensional (3D) imaging presents a more appropriate method to visualize the vascular architecture in tissue. Here we describe the complete protocol that we use to characterize the vasculature of different organs in mice encompassing the methods to fluorescently label vessels, optically clear tissue, collect 3D vascular images, and quantify these vascular images with a semi-automated approach. To validate the automated segmentation of vascular images, one user manually segmented one hundred random regions of interest across different vascular images. The automated segmentation results had an average sensitivity of 83±11% and an average specificity of 91±6% when compared to manual segmentation. Applying this procedure of image analysis presents a method to reliably quantify and characterize vascular networks in a timely fashion. This procedure is also applicable to other methods of tissue clearing and vascular labels that generate 3D images of microvasculature.

Introduction

The microvasculature facilitates gas exchange, provides nutrients to cells, and regulates blood flow in response to stimuli [1]. Thus, it plays a fundamental role in the survival and health of tissues and organs. Vascular abnormalities indicate pathology for various conditions, such as

analysis, decision to publish, or preparation of the manuscript.

Competing interests: The authors have declared that no competing interests exist.

compromised vessel integrity in cerebral microvascular disease and angiogenesis in tumors [2–4]. In addition, impaired blood flow to the brain is associated with neurodegenerative disorders such as Alzheimer's disease [5, 6]. Traditional immunohistochemistry enables the visualization of tissue cross-sections containing exogenously labeled vasculature. Although this approach quantifies vascular changes within small fields of view, more practical ways exist to study the vasculature on the scale of whole organs. Furthermore, traditional immunohistochemistry requires tissue sectioning into thin (6–40 μm) sections, which effectively limits visualization of features to planar views and thus impedes facile 3D visualization of vascular architecture.

Volumetric imaging of tissue samples is vital to studying the microvasculature in its native state. The main limitation of 3D imaging of tissue samples is optical scattering resulting from the microscopic variations of refractive index occurring in most biological tissues. Organic and aqueous solvents reduce tissue turbidity by achieving refractive index matching [7, 8]. CLARITY is a popular tissue clearing method involving embedding of the sample into a hydrogel and using an electric current to remove lipids from the sample [9]. Other tissue clearing procedures have advantages and disadvantages associated with clearing time, the extent of clearing, and preservation of original tissue characteristics (e.g. size, endogenous fluorescence).

Quantitative analysis of microvasculature is essential to understand how structural variations in the microvascular network may change for different pathological states [10]. The feasibility of such analysis depends on accurate, ideally automated segmentation methods for isolating the microvasculature from the background due to the hundreds of gigabytes of data generated with high-resolution 3D imaging. Various groups have developed automated algorithms to perform quantitative characterization of vascular images [11, 12]. However, each method varies in complexity, processing time, and computational requirements.

We currently use iDISCO (immunolabeling-enabled three-dimensional imaging of solvent-cleared organs) as our primary tissue clearing method [7, 13]. Briefly, iDISCO consists of methanol dehydration, lipid removal with dichloromethane, and refractive index matching with dibenzyl ether. iDISCO is a fast, simple-to-implement clearing method that enables deep-tissue imaging. It is compatible with many exogenous labels often used for traditional immunohistochemistry. We previously demonstrated the effectiveness of iDISCO in combination with lectin-DyLight-649 for 3D visualization of vasculature in a mouse brain [13]. We also used Prussian blue labeling of hemosiderin [14–16], a by-product of cerebral microhemorrhages, with iDISCO-cleared brains and lectin-DyLight-649 labeling.

In this paper, we first review different methods for vascular labeling in conjunction with optical clearing that other groups have published. Next, we describe our complete protocol for imaging the vasculature in different organs in mice (Fig 1A). Specifically, we report on sample collection and perfusion of lectin-DyLight-649 followed by adding additional labels as desired and optical clearing. We then describe our procedure to obtain 3D confocal microscopy images. Finally, we describe our semi-automated approach to process the resulting images and quantify the vascular architecture in three dimensions. The proposed methodology consists of simple procedures that require minimal computational resources, which enables other researchers to produce accurate three-dimensional vascular images.

Vascular imaging with various vessel labels and optical clearing techniques

Reviewing the literature on 3D vascular imaging of cleared tissue will show the large variability in methodology across different experiments (see Table 1 for specific references). For example, blood vessels can be visualized with transgenic animals expressing a fluorescent protein in

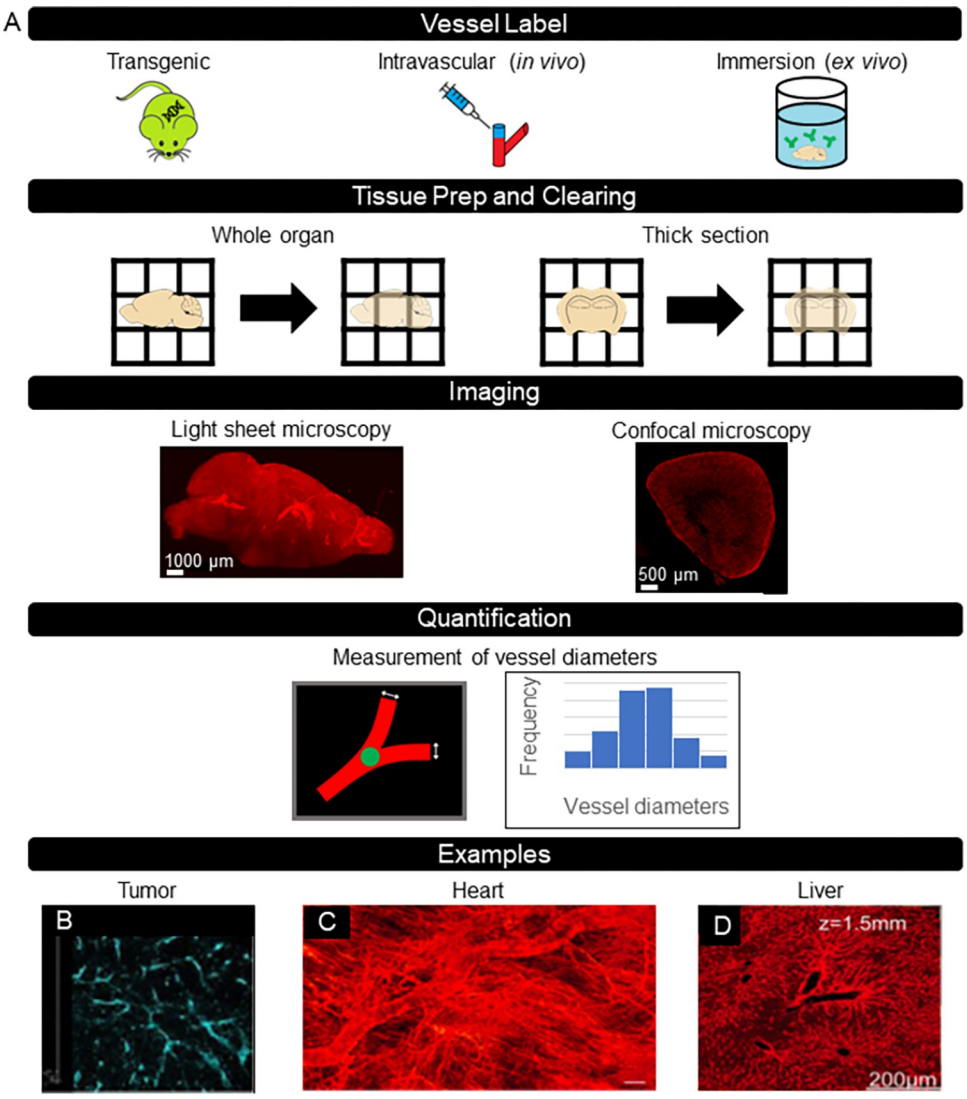

Fig 1. Overview of protocol for vascular visualization and quantification with various examples published in literature. A) Illustrations of the critical steps and workflow for vascular visualization in cleared tissue. B-D) Examples of vascular visualization in literature. B) Visualization of CD31-labeled mouse tumor vasculature with seeDB [30]. C) Visualization of DiI-labeled mouse heart vasculature with FocusClear [11]. D) Visualization of liver vasculature from *Tie2-Cre* mouse model with PEGASOS [33].

https://doi.org/10.1371/journal.pone.0289109.g001

endothelial cells, labeled *in vivo* with intravascular dyes, or labeled *ex vivo* with immersion-based antibody labeling. In addition, tissue preparation can vary from thick tissue sections and whole organs to whole-mount specimens, depending on the purpose of an experiment. Finally, clearing procedures can be grouped into aqueous solvents [17–22], organic solvents [12, 23–25], and hydrogel-based [26–29].

When selecting a clearing procedure, it is essential to consider its compatibility with the chosen vascular label. Endogenous fluorescence intensity is known to be reduced when using the iDISCO protocol; hence, an alternative vascular label would be preferred. Imaging of cleared samples is typically performed with confocal microscopy or light-sheet microscopy. Lastly, vascular-related metrics, such as vessel diameters and vessel density, are quantified with existing software such as FIJI and Imaris or custom-designed software such as ClearMap 2.0.

Table 1. Summary of different approaches to visualizing 3D microvasculature in optically cleared tissues.

Clearing agent(s)	Organ(s)	Vascular label	Quantification Method/Tool	Quantified Metrics
iDISCO [7]	brain, peripheral nervous system, kidney, muscle, heart, whisker pad, entire embryo	PeCAM	N/A	N/A
iDISCO [12]	brain	CD31, podocalyxin, collagen IV, smooth muscle actin, transgelin, von Willebrand factor	ClearMap 2.0, TubeMap	vascular density, vascular organization, vascular remodeling
MACS [17]	brain, heart, lung, spleen, femur, kidney, spinal cord, embryo, entire body	DiI, tetramethylrhodamine-conjugated dextran	Custom algorithm via Python, Imaris: surface function	glomerulus number and glomerulus volume; general metrics (imaging depth, size change, fluorescence intensity)
Sca*l*eS [18]	brain	Texas Red lectin	custom C++, commercial Volocity, commercial Igor Pro	microglia and Aβ plaques with custom C++, distance between microglia and Aβ plaques
CUBIC, BABB [19]	heart	FITC-lectin, 649-lectin, CD31	N/A	N/A
Sca*l*eS [20]	pancreas	lectin-DyLight	N/A	N/A
FocusClear [21]	small intestine	DiI	N/A	N/A
FocusClear, ScaleSQ, RIMS, sRIMS [22]	brain	Lectin-Dylight649	MATLAB	optical properties, vascular density
FDISCO [23]	brain, kidney	AlexaFluor647, CD31, lectin-DyLight-649	Imaris, ImageJ	general metrics (size change, imaging depth, fluorescence quantification)
3DISCO [24]	brain	FITC albumin-gelatin hydrogel	Imaris, ImageJ	vessel density, vessel diameter
vDISCO [25]	whole mouse	GFP, lectin	ImageJ, ClearMap	signal level, microglia distribution
CLARITY, TDE [26]	brain	lectin-FITC, gel-BSA-FITC, gel-BSA-TRITC	Markov random field-based algorithm, ImageJ, Amira 5.3 software	automatic segmentation, vessel diameter, vessel length
CLARITY [27]	brain	fluorescein-conjugated tomato lectin	Amira	area, volume, perimeter, and length of stained vessel
X-CLARITY [28]	placenta	DiI	Imaris, Image-Pro Premier	N/A
CLARITY [29]	retina	Griffonia lectin	Angiotool, ImageJ, Vaa3D, MATLAB, APP-2.0	network tracing, vessel percentage area, total number of junctions, junction density, total vessel length, average vessel length, total number of endpoints, mean lacunarity
PEGASOS [33]	whole mouse	αSMA, GS-IB4 isolectin dye, collagen IV	Imaris	vessel density
SeeDB, SeeDB2, 3DISCO, uDISCO, iDISCO, CUBIC, simplified CLARITY method, 75% v/v glycerol, Ce3D, FRUIT [34]	lymph nodes	CD31	Imaris: surface function, ImageJ	general metrics (imaging depth, size change, fluorescence intensity)
sodium dodecyl sulfate/ sodium deoxycholate with Sca*l*eCUBIC-2 [35]	brain	RITC-Dex-GMA, Texas red lectin, CD31, αSMA	N/A	capillary diameters, signal-to-noise ratio
iDISCO with CUBIC [36]	ovary	endomucin	N/A	N/A
thiazone with PEG-400 [37]	dorsal skin	N/A (imaged blood flow via LSI)	N/A	blood flowblood flow via LSCI
iDISCO [38]	brain	Dye-conjugated secondary antibodies	ClearMap	Aβ deposits
FACT [39]	brain, spinal cord, heart, lung, adrenal gland, pancreas, liver, esophagus, duodenum, jejunum, ileum, muscle, bladder, ovary, uterus	CD31, autofluorescence	Imaris	segmentation

(*Continued*)

Table 1. (Continued)

Clearing agent(s)	Organ(s)	Vascular label	Quantification Method/Tool	Quantified Metrics
BABB [40]	heart	PECAM1	N/A	N/A
DBE, SCALE, CLARITY, CUBIC [41]	heart and embryo	GFP		
3DISCO [42]	brain	tomato lectin	N/A	N/A
CLARITY with ScaleA2 [43]	ovary, uterus, lung, liver	tdTomato	Ilastik, Imaris	segmentation, total vessel length, vessel mean diameter, vessel straightness, total number of branching points
ethyl-cinnamate [44]	liver, skin, lungs, heart, muscles, pancreas, brain, kidney	In-house developed NIR fluorescent dye (MHI148-PEI)	Leica LAS X	segmentation, volume of glomerulus
CLARITY, iDISCO [45]	brain	lectin-DyLight, lectin-FITC, anti-CD31	Imaris, segmentation	number of branches, total vessel length, total vessel volume, total vessel area, diameter of single segments per volume, distance between cells and nearest vessel
PEGASOS [46]	bone, teeth	tdTomato	Imaris	blood vessel volume
No clearing approach [47]	retina, heart	DiI	N/A	N/A
FRUIT 100 [48]	brain tumor	DiI	N/A	N/A
FocusClear [49]	brain	DiI	N/A	optical properties
FocusClear [50]	brain	DiI	MATLAB	functional vascular density

https://doi.org/10.1371/journal.pone.0289109.t001

We have reviewed several optical clearing methods utilized to image vasculature. They are organized in Table 1 by clearing method, tissue type, vessel label, and quantification. Vascular images in cleared tissue from select publications are included in Fig 1B–1D. Lee et al. (2017) demonstrated the ability to use seeDB, a water-based clearing method that relies on fructose, to visualize CD31-labeled endothelial cells in whole mouse tumors (Fig 1B, 1B') [30, 31]. Our group visualized vessels with an intravascular fluorescent dye and FocusClear (Fig 1C, 1C') [11]. In addition, we quantified functional vascular density in different regions of cardiac tissue with a custom MATLAB algorithm [11, 32]. With a polyethylene glycol-associated solvent system (PEGASOS), researchers developed a clearing technique that preserved both hard and soft tissue structures (Fig 1D, 1D') [33], allowing for vascular imaging throughout an entire specimen.

Three-dimensional quantitative analysis of microvasculature imaged in thick tissue sections

Microvascular labeling is performed by injecting of a lectin conjugated to a fluorophore. In our work, we have focused on the DyLight-649 fluorophore. As the lectin travels through the circulatory system, it binds to glycoproteins adjacent to endothelial cells of the vascular wall. This binding allows for the labeling of the vascular network within every organ of the body.

An overview of our workflow is outlined below in Fig 2. First, we administer lectin-DyLight-649 via retroorbital injection. The lectin is allowed to circulate throughout the body before cardiac perfusion with saline, followed by formalin. Mouse brains are then extracted, bisected into hemispheres, and sectioned into thick (0.5–1.0mm) sections. Each section is then imaged using confocal microscopy to generate image stacks of the complete section throughout its entire thickness. Next, segmentation is performed by a custom MATLAB (MathWorks, Natick, MA) script. Finally, neuTube, an open-source neuron tracing software, is used to extract diameter measurements of the vessel structures [51].

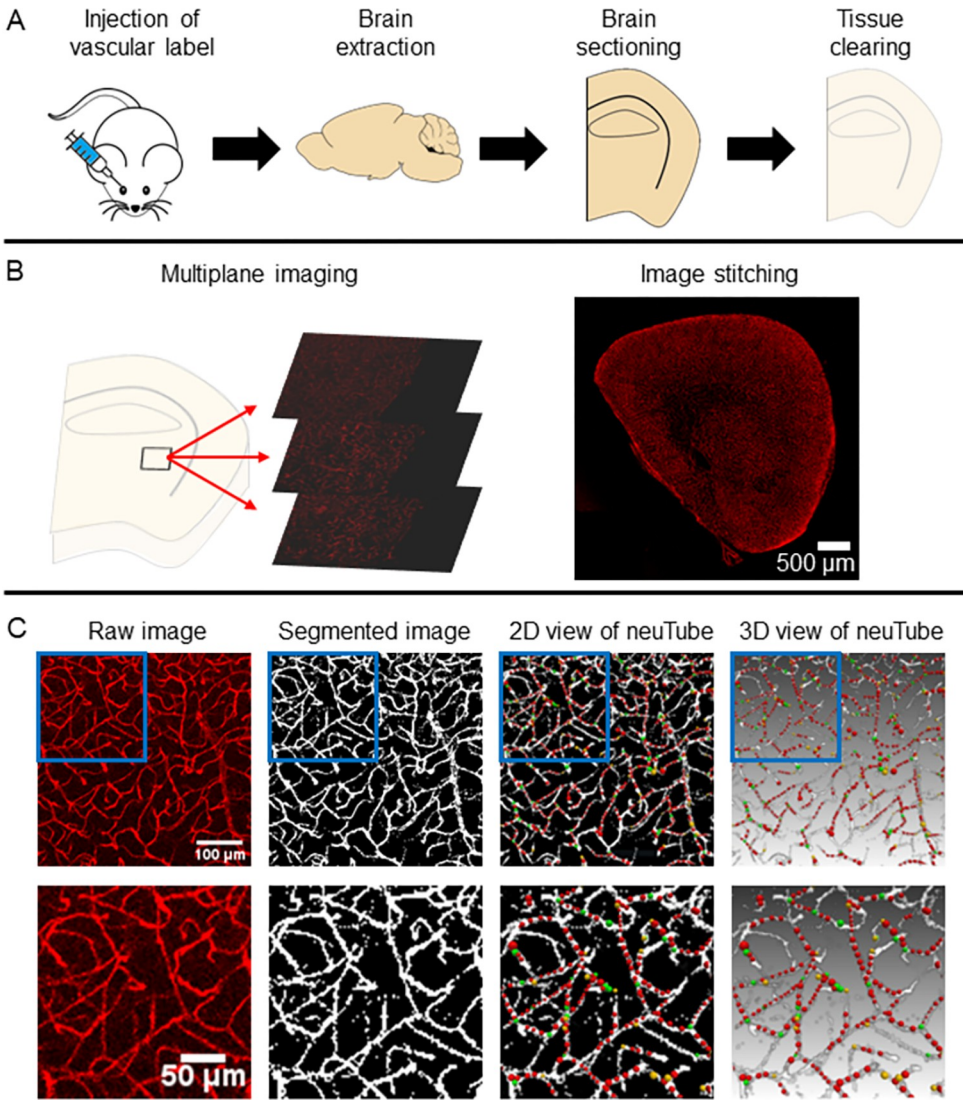

Fig 2. Workflow for 3D visualization and quantitation of microvasculature in thick tissue sections. A) Vasculature is labeled via retroorbital injection of lectin-DyLight-649. Brains are then sectioned and cleared. B) Depiction of multiplane imaging and image stitching to visualize an entire sample in 3D via confocal microscopy. C) From left to right: representative example of a raw image of the vasculature, segmented vasculature via MATLAB, 2D view of traced vasculature via neuTube, and 3D view of traced vasculature via neuTube.

https://doi.org/10.1371/journal.pone.0289109.g002

Materials and methods

The protocol described in this article is published on protocols.io (https://doi.org/10.17504/protocols.io.j8nlkk7m1l5r/v1) and is included as S1 File. All custom-written MATLAB code is available upon reasonable request made to the corresponding author.

Animals

This work was in compliance with protocols approved by the University of California, Irvine Institutional Animal Care and Use Committee (approval number: AUP-19-084, AUP-19-032). Anesthesia is induced at 4% isoflurane within a chamber and maintained at 1.5% isoflurane. Euthanasia is performed via cardiac perfusion under 4% isoflurane anesthesia.

Anticipated results

The procedures detailed herein present a simple method for producing optically cleared (> 1 mm thick) tissue samples with fluorescently labeled vasculature. Samples can then be imaged to generate 3D images of the microvasculature. The described segmentation method using custom MATLAB scripts and neuTube presents an automated method to convert the fluorescent images into binary images. The binary images can then be used to characterize microvasculature by quantifying vessel density and vessel sizes. The procedures here can be enhanced by using additional histology dyes or immunohistochemistry to label biomarkers or other structures of interest in tissue. In doing so, one can visualize and quantify the microvasculature surrounding these biomarkers to gain insight into their relationship.

Validation

Segmentation results

To validate the accuracy of our automatically segmented images, manually segmented images were created to serve as a ground truth comparison. One author (DFX) used MATLAB to manually outline every pixel within an ROI of an image that the author determined to belong to a vessel. Each ROI (n = 100) was presented as a maximum intensity projection (MIP) image of a 50x50x5 voxel (113x113x38 μm) region. A MIP is used to present a 2D image that is more feasible for manual tracing. The corresponding 50x50x5 voxel region MIP from the automated segmented image was compared. Four representative examples of this are depicted in Fig 3. Across the 100 ROIs, the average sensitivity was 83±11%, and the average specificity was 91 ±6%. The Dice similarity coefficient between manually segmented and automated segmented images was calculated across all ROIs. This coefficient can measure similarity between two sets of Boolean data and ranges between 0 and 1, where 1 represents identical data, and 0 represents opposite data [52]. The average Dice similarity coefficient across 100 ROIs was 0.74 ±0.09.

Diameter results with neuTube

Manually measured diameters of individual vessels were used as a ground truth comparison for neuTube approximated vessel diameters. Images from various brain sections across three different animals were used. One author (DFX) was presented with a randomly generated 50x50x5 voxel (113x113x38 μm) size region as a MIP. Within the image, the user was tasked with using MATLAB to estimate the diameter of a single vessel in the image at five different points along the vessel by drawing lines approximately perpendicular to the vessel's centerline. In neuTube, five nodes along the corresponding vessel were selected. The average of the five manual diameter measurements via MATLAB and the five automated diameter measurements via neuTube were compared. Two representative examples of this are depicted in Fig 4A. The absolute difference between diameter measurements was 1.16±0.73 μm as shown in Fig 4B (n = 50 vessels of diameters ranging from 1.78 μm to 3.19 μm).

Discussion

Due to the understood importance of cerebrovascular architecture to brain function, several groups have reported on similar methods to what we report here. Lugo-Hernandez et al. (2017) use an injected fluorescent-labeled hydrogel, the 3DISCO optical clearing approach, and light-sheet microscopy to image the vasculature, but vascular analysis is performed using a commercial software package (Imaris), which uses both user intervention and proprietary algorithms to achieve binary vascular maps [24]. Di Giovanna et al. (2018) employed a

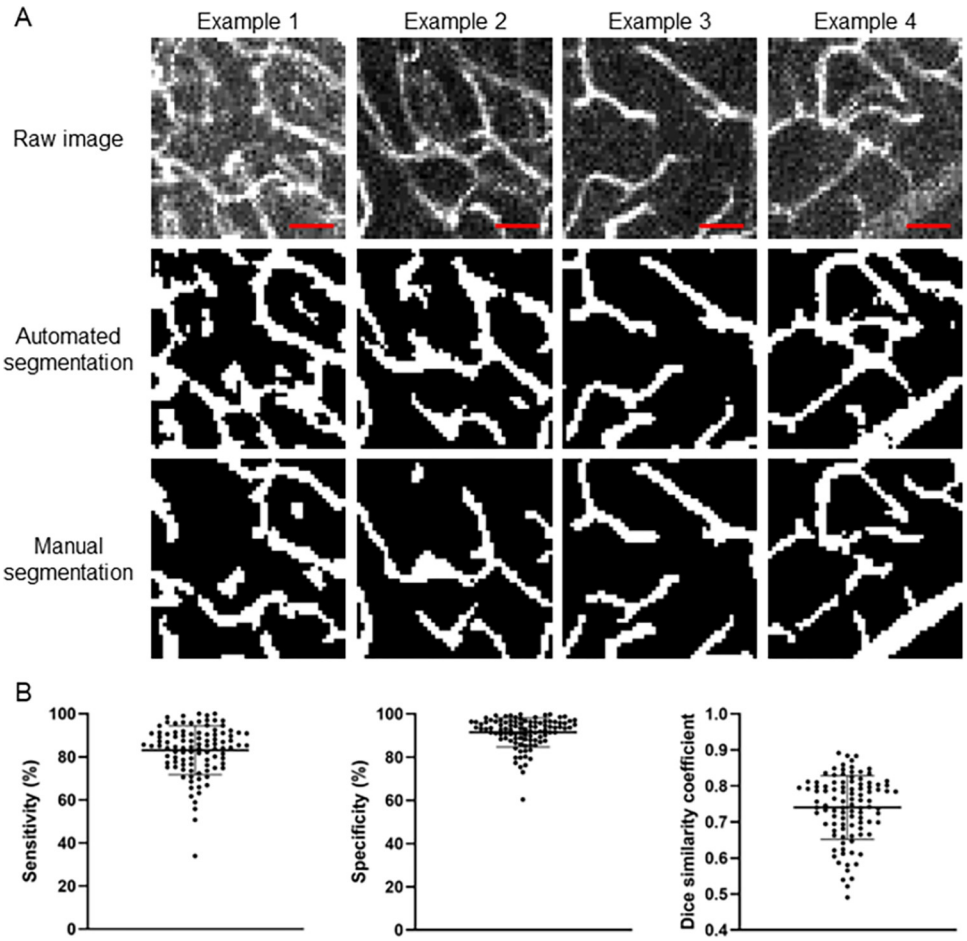

Fig 3. Representative examples of raw images, automated segmentation, and manual segmentation. A) Automated segmentation is performed using the iterative selection method as described in the step-by-step protocol (see S1 File). Manual segmentation is performed by manual tracing of vessels. Each example shown is a 50x50 pixel region from a different brain section. Scale bar is 25 μm. B) Comparison of vessel pixels identified via manual segmentation (ground truth) and automated segmentation. The sensitivity, specificity, and Dice similarity coefficient of all 100 ROIs are shown in the graph. The average sensitivity was 83±11%, the average specificity was 91±6%, and the average Dice similarity coefficient was 0.74±0.09.

https://doi.org/10.1371/journal.pone.0289109.g003

fluorescent gel perfusion approach to fill the vasculature, CLARITY-based optical clearing, and light-sheet microscopy; they describe the use of an automatic segmentation method based on a Markov random field, but enabling details of the algorithm are not provided [26]. Quintana et al. (2019) and Wälchli et al. (2021) used a vascular corrosion cast approach and micro-computerized tomography to visualize the whole-brain vasculature with exquisite detail, along with automated thresholding approaches (including the same iterative selection method we describe here); however, this approach requires access to a micro-CT system, and its compatibility with fluorescence labels requires further investigation [53, 54]. Kirst et al. (2020) report on the combination of immunolabeling, iDISCO-based optical clearing, and light-sheet microscopy to achieve whole-brain three-dimensional maps of the cerebrovasculature. They provide a sophisticated open-source software package to create binary maps of the vasculature, but a high-performance dedicated workstation is required to execute their computationally-intensive approach [12]. Hahn et al. (2021) used the same lectin-Dylight-649 fluorophore as we describe here, along with the FluoClearBABB optical clearing approach and light-sheet

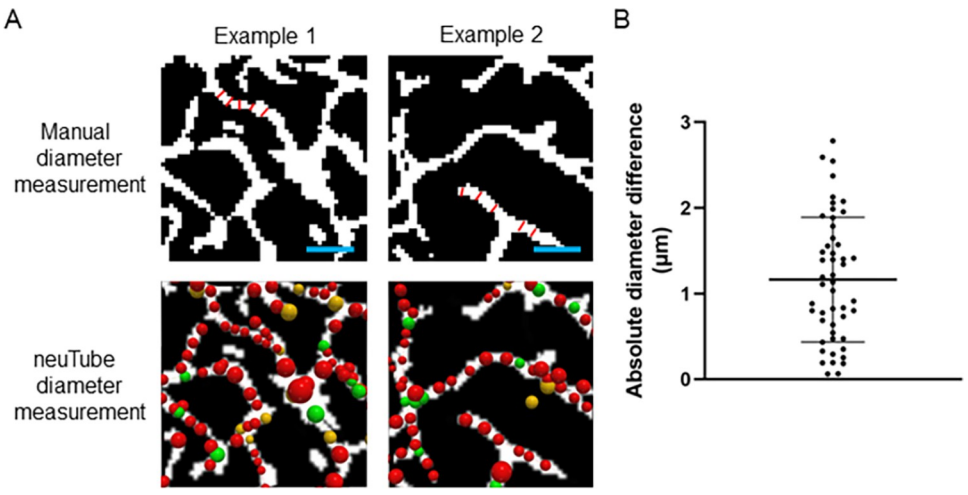

Fig 4. Two representative examples of manual diameter measurements and neuTube diameter measurements. A) Within a 50x50 pixel region, one vessel is chosen by the user for analysis. The manual diameter measurement is determined by drawing a line approximately perpendicular to the centerline of the vessel at 5 locations (shown with red lines in the top row of images). The manual diameter measurement for a given vessel is the average of these 5 measurements. The same vessel is identified within the automated neuTube output where each node (shown as a sphere in the bottom row of images) represents the diameter determined by neuTube at that location in the image. The neuTube diameter measurement for a given vessel is recorded as the average of five nodes along that vessel Scale bar is 25 μm. B) The absolute difference in diameter between manual measurement and neuTube measurement for 50 different vessels is shown. The mean difference was 1.16±0.73 μm.

https://doi.org/10.1371/journal.pone.0289109.g004

microscope; they describe an automated image analysis approach using a trained random forest classification scheme "ilastik" (Berg et al. 2019) [55, 56]. Takahashi et al. (2022) used the Cre/lox approach to induce Td tomato expression in endothelial cells, and combined this with CUBIC-based optical clearing and light-sheet microscopy to image the vasculature; they too used the ilastik software module for analysis [57]. Zhu et al. (2022) used different combinations of vascular labels and optical clearing approaches with light-sheet microscopy, but they also used Imaris for vascular image analysis [58].

With the work described here, we focused on describing the entire process of vessel labeling, brain extraction, and quantitative image analysis, on enabling other researchers to integrate and expand upon our protocol into their individualized workflow. We acknowledge that other vessel segmentation approaches may offer advantages to our approach described here, and the vetting of those approaches will be the subject of future work. Here, we emphasize the transparency of our methodology and ease of implementation of each step, with minimal computational resources, to achieve an approach that can rapidly yield accurate three-dimensional vascular maps. The vessel segmentation approach readily works with similarly-prepared whole brains imaged with light-sheet microscopy [13].

There are several potential applications for the methods described here. As angiogenesis occurs in organs, endothelial cells respond to local signals to adapt vessels to the surrounding environment [59]. Angiogenesis plays an essential role in tumor formation. In tumors, angiogenesis directly impacts tumor growth and metastasis. Overexpression of proangiogenic factors leads to uncontrolled vascular growth in tumors [60]. As a result, anti-angiogenic drugs are frequently used as a potential treatment option for cancer. Lectin-DyLight-649 combined with iDISCO presents a robust procedure for labeling the microvasculature in all body areas, including tumors. Changes in vessel density, tortuosity, and diameters can be quantified to evaluate the efficacy of novel anti-angiogenic treatments.

Ischemic strokes occur when there is a significant drop in cerebral blood flow due to occlusion in a cerebral artery. A major consequence of such an event is necrosis of neurons due to a deficient blood supply [61]. A method to visualize the microvascular network and the surrounding neurons, astrocytes, and glial cells can provide a detailed 3D snapshot of the brain in response to an ischemic stroke and monitor potential treatments over time.

In addition to visualizing cerebral microhemorrhages within the surrounding microvascular network and providing the improved capability to estimate the size range of these lesions, our approach can provide enhanced imaging for other disease entities. For example, a growing body of literature suggests a contribution of dysfunctional regulation of cerebral blood flow and various types of cognitive impairment [5]. The ability to visualize the cerebral microvasculature in three dimensions offers a new gateway, potentially leading to the identification of novel treatment targets for neurological disorders.

Supporting information

S1 File. Step-by-step protocol, also available on protocols.io. (https://www.protocols.io/private/653D11CD1E6A11ED93350A58A9FEAC02).
(PDF)

Acknowledgments

This study was made possible in part through access to the Optical Biology Core Facility of the Developmental Biology Center, a shared resource supported by the Cancer Center Support Grant (CA-62203) and Center for Complex Biological Systems Support Grant (GM-076516) at the University of California, Irvine.

Author Contributions

Conceptualization: Krystal LoPresti, Yuke Wang, Christopher Robinson, Bernard Choi.

Data curation: Danny F. Xie.

Formal analysis: Danny F. Xie, Krystal LoPresti, Bernard Choi.

Funding acquisition: David H. Cribbs, Mark Fisher, Bernard Choi.

Investigation: Danny F. Xie, Krystal LoPresti, Yuke Wang, Christopher Robinson, Chuo Fang.

Methodology: Danny F. Xie, Christian Crouzet, Bernard Choi.

Project administration: Bernard Choi.

Resources: Chuo Fang, David H. Cribbs, Mark Fisher, Bernard Choi.

Software: Danny F. Xie, Krystal LoPresti, Bernard Choi.

Supervision: Christian Crouzet, Bernard Choi.

Visualization: Danny F. Xie, Krystal LoPresti, William Jones, Fjolla Muqolli, Bernard Choi.

Writing – original draft: Danny F. Xie, Krystal LoPresti, Yuke Wang, Christopher Robinson, Bernard Choi.

Writing – review & editing: Danny F. Xie, Christian Crouzet, Krystal LoPresti, Yuke Wang, Christopher Robinson, William Jones, Fjolla Muqolli, Chuo Fang, David H. Cribbs, Mark Fisher, Bernard Choi.

References

1. Jacob M, Chappell D, Becker BF. Regulation of blood flow and volume exchange across the microcirculation. Crit Care. 2016; 20(1):1–13. Available from: https://doi.org/10.1186/s13054-016-1485-0 PMID: 27765054
2. Carmeliet P, Jain RK. Molecular mechanisms and clinical applications of angiogenesis. Nature. 2011 May 18; 473(7347):298–307. Available from: https://doi.org/10.1038/nature10144 PMID: 21593862
3. Haller S, Vernooij MW, Kuijer JPA, Larsson EM, Jäger HR, Barkhof F. Cerebral Microbleeds: Imaging and Clinical Significance. Radiology. 2018 Apr; 287(1):11–28. Available from: https://doi.org/10.1148/radiol.2018170803 PMID: 29558307
4. Fang C, Magaki SD, Kim RC, Kalaria RN, Vinters H V., Fisher M. Arteriolar neuropathology in cerebral microvascular disease. Neuropathol Appl Neurobiol. 2023 Feb; 49(1):1–18. Available from: https://doi.org/10.1111/nan.12875 PMID: 36564356
5. Sweeney MD, Kisler K, Montagne A, Toga AW, Zlokovic B V. The role of brain vasculature in neurodegenerative disorders. Nat Neurosci. 2018; 21(10):1318–31. Available from: https://doi.org/10.1038/s41593-018-0234-x PMID: 30250261
6. Lugano R, Ramachandran M, Dimberg A. Tumor angiogenesis: causes, consequences, challenges and opportunities. Cell Mol Life Sci. 2020; 77(9):1745–70. Available from: https://doi.org/10.1007/s00018-019-03351-7 PMID: 31690961
7. Renier N, Wu Z, Simon DJ, Yang J, Ariel P, Tessier-Lavigne M. IDISCO: A simple, rapid method to immunolabel large tissue samples for volume imaging. Cell. 2014; 159(4):896–910. Available from: https://doi.org/10.1016/j.cell.2014.10.010 PMID: 25417164
8. Susaki EA, Tainaka K, Perrin D, Kishino F, Tawara T, Watanabe TM, et al. Whole-brain imaging with single-cell resolution using chemical cocktails and computational analysis. Cell. 2014; 157(3):726–39. Available from: https://doi.org/10.1016/j.cell.2014.03.042 PMID: 24746791
9. Chung K, Wallace J, Kim SY, Kalyanasundaram S, Andalman AS, Davidson TJ, et al. Structural and molecular interrogation of intact biological systems. Nature. 2013 May 16; 497(7449):332–7. Available from: https://doi.org/10.1038/nature12107 PMID: 23575631
10. Kalaria RN, Akinyemi R, Ihara M. Stroke injury, cognitive impairment and vascular dementia. Biochim Biophys Acta—Mol Basis Dis. 2016 May; 1862(5):915–25. Available from: https://doi.org/10.1016/j.bbadis.2016.01.015 PMID: 26806700
11. Moy AJ, Lo PC, Choi B. High-resolution visualization of mouse cardiac microvasculature using optical histology. Biomed Opt Express. 2014 Jan 1; 5(1):69. Available from: https://doi.org/10.1364/BOE.5.000069 PMID: 24466477
12. Kirst C, Skriabine S, Vieites-Prado A, Topilko T, Bertin P, Gerschenfeld G, et al. Mapping the Fine-Scale Organization and Plasticity of the Brain Vasculature. Cell. 2020; 180(4):780–795.e25. Available from: https://doi.org/10.1016/j.cell.2020.01.028 PMID: 32059781
13. Khouri K, Xie DF, Crouzet C, Bahani AW, Cribbs DH, Fisher MJ, et al. Simple methodology to visualize whole-brain microvasculature in three dimensions. Neurophotonics. 2021 Apr 19; 8(02):1–10. Available from: https://doi.org/10.1117/1.NPh.8.2.025004 PMID: 33884280
14. Crouzet C, Jeong G, Chae RH, LoPresti KT, Dunn CE, Xie DF, et al. Spectroscopic and deep learning-based approaches to identify and quantify cerebral microhemorrhages. Sci Rep. 2021 Dec 21; 11(1):10725. Available from: https://doi.org/10.1038/s41598-021-88236-1 PMID: 34021170
15. Lo P, Crouzet C, Vasilevko V, Choi B. Visualization of microbleeds with optical histology in mouse model of cerebral amyloid angiopathy. Microvasc Res. 2016; 105:109–13. Available from: https://doi.org/10.1016/j.mvr.2016.02.002 PMID: 26876114
16. Sumbria RK, Grigoryan MM, Vasilevko V, Paganini-Hill A, Kilday K, Kim R, et al. Aging exacerbates development of cerebral microbleeds in a mouse model. J Neuroinflammation. 2018 Dec 6; 15(1):69. Available from: https://doi.org/10.1186/s12974-018-1092-x PMID: 29510725
17. Zhu J, Yu T, Li Y, Xu J, Qi Y, Yao Y, et al. MACS: Rapid Aqueous Clearing System for 3D Mapping of Intact Organs. Adv Sci. 2020 Apr 25; 7(8):1903185. Available from: https://doi.org/10.1002/advs.201903185 PMID: 32328422
18. Hama H, Hioki H, Namiki K, Hoshida T, Kurokawa H, Ishidate F, et al. ScaleS: an optical clearing palette for biological imaging. Nat Neurosci. 2015 Oct 14; 18(10):1518–29. Available from: https://doi.org/10.1038/nn.4107 PMID: 26368944
19. Nehrhoff I, Ripoll J, Samaniego R, Desco M, Gómez-Gaviro MV. Looking inside the heart: a see-through view of the vascular tree. Biomed Opt Express. 2017 Jun 1; 8(6):3110. Available from: https://doi.org/10.1364/BOE.8.003110 PMID: 28663930

20. Nishimura W, Sakaue-Sawano A, Takahashi S, Miyawaki A, Yasuda K, Noda Y. Optical clearing of the pancreas for visualization of mature β-cells and vessels in mice. Islets. 2018 May 4; 10(3):e1451282. Available from: https://doi.org/10.1080/19382014.2018.1451282 PMID: 29617192

21. Fu YY, Tang SC. Optical clearing facilitates integrated 3D visualization of mouse ileal microstructure and vascular network with high definition. Microvasc Res. 2010; 80(3):512–21. Available from: https://doi.org/10.1016/j.mvr.2010.06.003 PMID: 20600164

22. Loren M, Crouzet C, Bahani A, Vasilevko V, Choi B. Optical clearing potential of immersion-based agents applied to thick mouse brain sections. PLoS One. 2019 May 10; 14(5):e0216064. Available from: https://doi.org/10.1371/journal.pone.0216064 PMID: 31075111

23. Qi Y, Yu T, Xu J, Wan P, Ma Y, Zhu J, et al. FDISCO: Advanced solvent-based clearing method for imaging whole organs. Sci Adv. 2019 Jan 4; 5(1):1–14. Available from: https://doi.org/10.1126/sciadv.aau8355 PMID: 30746463

24. Lugo-Hernandez E, Squire A, Hagemann N, Brenzel A, Sardari M, Schlechter J, et al. 3D visualization and quantification of microvessels in the whole ischemic mouse brain using solvent-based clearing and light sheet microscopy. J Cereb Blood Flow Metab. 2017 Oct 28; 37(10):3355–67. Available from: https://doi.org/10.1177/0271678X17698970 PMID: 28350253

25. Cai R, Pan C, Ghasemigharagoz A, Todorov MI, Förstera B, Zhao S, et al. Panoptic imaging of transparent mice reveals whole-body neuronal projections and skull–meninges connections. Nat Neurosci. 2019; 22(2):317–27. Available from: https://doi.org/10.1038/s41593-018-0301-3 PMID: 30598527

26. Di Giovanna AP, Tibo A, Silvestri L, Müllenbroich MC, Costantini I, Allegra Mascaro AL, et al. Whole-Brain Vasculature Reconstruction at the Single Capillary Level. Sci Rep. 2018 Aug 22; 8(1):12573. Available from: https://doi.org/10.1038/s41598-018-30533-3 PMID: 30135559

27. Krolewski DM, Kumar V, Martin B, Tomer R, Deisseroth K, Myers RM, et al. Quantitative validation of immunofluorescence and lectin staining using reduced CLARITY acrylamide formulations. Brain Struct Funct. 2018 Mar 14; 223(2):987–99. Available from: https://doi.org/10.1007/s00429-017-1583-z PMID: 29243106

28. Carrillo M, Chuecos M, Gandhi K, Bednov A, Moore DL, Maher J, et al. Optical tissue clearing in combination with perfusion and immunofluorescence for placental vascular imaging. Medicine (Baltimore). 2018 Sep; 97(39):e12392. Available from: https://doi.org/10.1097/MD.0000000000012392 PMID: 30278515

29. Singh JN, Nowlin TM, Seedorf GJ, Abman SH, Shepherd DP. Quantifying three-dimensional rodent retina vascular development using optical tissue clearing and light-sheet microscopy. J Biomed Opt. 2017 Jul 18; 22(07):1. Available from: https://doi.org/10.1117/1.JBO.22.7.076011 PMID: 28717817

30. Lee SS young Bindokas VP, Kron SJ. Multiplex three-dimensional optical mapping of tumor immune microenvironment. Sci Rep. 2017;(November):1–11. Available from: https://doi.org/10.1038/s41598-017-16987-x PMID: 29208908

31. Ke M tsen, Fujimoto S, Imai T. SeeDB: a simple and morphology-preserving optical clearing agent for neuronal circuit reconstruction. Nat Neurosci. 2013 Aug 23; 16(8):1154–61. Available from: https://doi.org/10.1038/nn.3447 PMID: 23792946

32. White SM, George SC, Choi B. Automated computation of functional vascular density using laser speckle imaging in a rodent window chamber model. Microvasc Res. 2011; 82(1):92–5. Available from: https://doi.org/10.1016/j.mvr.2011.03.006 PMID: 21419785

33. Jing D, Zhang S, Luo W, Gao X, Men Y, Ma C, et al. Tissue clearing of both hard and soft tissue organs with the pegasos method. Cell Res. 2018; 28(8):803–18. Available from: https://doi.org/10.1038/s41422-018-0049-z PMID: 29844583

34. Matryba P, Sosnowska A, Wolny A, Bozycki L, Greig A, Grzybowski J, et al. Systematic Evaluation of Chemically Distinct Tissue Optical Clearing Techniques in Murine Lymph Nodes. J Immunol. 2020 Mar 1; 204(5):1395–407. Available from: https://doi.org/10.4049/jimmunol.1900847 PMID: 31953352

35. Miyawaki T, Morikawa S, Susaki EA, Nakashima A, Takeuchi H, Yamaguchi S, et al. Visualization and molecular characterization of whole-brain vascular networks with capillary resolution. Nat Commun. 2020; 11(1):1–11. Available from: https://doi.org/10.1038/s41467-020-14786-z PMID: 32107377

36. McKey J, Cameron LA, Lewis D, Batchvarov IS, Capel B. Combined iDISCO and CUBIC tissue clearing and lightsheet microscopy for in toto analysis of the adult mouse ovary†. Biol Reprod. 2020 Apr 24; 102(5):1080–9. Available from: https://doi.org/10.1093/biolre/ioaa012 PMID: 31965156

37. Zhu D, Wang J, Zhi Z, Wen X, Luo Q. Imaging dermal blood flow through the intact rat skin with an optical clearing method. J Biomed Opt. 2010; 15(2):026008. Available from: https://doi.org/10.1117/1.3369739 PMID: 20459253

38. Liebmann T, Renier N, Bettayeb K, Greengard P, Tessier-Lavigne M, Flajolet M. Three-Dimensional Study of Alzheimer's Disease Hallmarks Using the iDISCO Clearing Method. Cell Rep. 2016; 16(4):1138–52. Available from: https://doi.org/10.1016/j.celrep.2016.06.060 PMID: 27425620

39. Khoradmehr A, Mazaheri F, Anvari M, Tamadon A. A Simple Technique for Three-Dimensional Imaging and Segmentation of Brain Vasculature U sing Fast Free-of-Acrylamide Clearing Tissue in Murine. Cell J. 2019 Apr; 21(1):49–56. Available from: https://doi.org/10.22074/cellj.2019.5684 PMID: 30507088

40. Ivins S, Roberts C, Vernay B, Scambler PJ. Analysis of Coronary Vessels in Cleared Embryonic Hearts. J Vis Exp. 2016 Dec 7; 2016(118):1–9. Available from: https://doi.org/10.3791/54800 PMID: 28060348

41. Kolesová H, Čapek M, Radochová B, Janáček J, Sedmera D. Comparison of different tissue clearing methods and 3D imaging techniques for visualization of GFP-expressing mouse embryos and embryonic hearts. Histochem Cell Biol. 2016 Aug 4; 146(2):141–52. Available from: https://doi.org/10.1007/s00418-016-1441-8 PMID: 27145961

42. Harrison CH, Buckland GR, Brooks SE, Johnston DA, Chatelet DS, Liu AKL, et al. A novel method to visualise the three-dimensional organisation of the human cerebral cortical vasculature. J Anat. 2018 Jun; 232(6):1025–30. Available from: https://doi.org/10.1111/joa.12805 PMID: 29520782

43. Oren R, Fellus-Alyagor L, Addadi Y, Bochner F, Gutman H, Blumenreich S, et al. Whole Organ Blood and Lymphatic Vessels Imaging (WOBLI). Sci Rep. 2018; 8(1):1–9. Available from: https://doi.org/10.1038/s41598-018-19663-w PMID: 29362484

44. Huang J, Brenna C, Khan A ul M, Daniele C, Rudolf R, Heuveline V, et al. A cationic near infrared fluorescent agent and ethyl-cinnamate tissue clearing protocol for vascular staining and imaging. Sci Rep. 2019 Dec 24; 9(1):521. Available from: https://doi.org/10.1038/s41598-018-36741-1 PMID: 30679514

45. Lagerweij T, Dusoswa SA, Negrean A, Hendrikx EML, de Vries HE, Kole J, et al. Optical clearing and fluorescence deep-tissue imaging for 3D quantitative analysis of the brain tumor microenvironment. Angiogenesis. 2017 Nov 11; 20(4):533–46. Available from: https://doi.org/10.1007/s10456-017-9565-6 PMID: 28699046

46. Yi Y, Men Y, Jing D, Luo W, Zhang S, Feng JQ, et al. 3-dimensional visualization of implant-tissue interface with the polyethylene glycol associated solvent system tissue clearing method. Cell Prolif. 2019 May 3; 52(3):e12578. Available from: https://doi.org/10.1111/cpr.12578 PMID: 30714253

47. Li Y, Song Y, Zhao L, Gaidosh G, Laties AM, Wen R. Direct labeling and visualization of blood vessels with lipophilic carbocyanine dye DiI. Nat Protoc. 2008 Nov 9; 3(11):1703–8. Available from: https://doi.org/10.1038/nprot.2008.172 PMID: 18846097

48. Peviani M, Spano G, Pagani A, Brugnara G, Covino C, Galli R, et al. Lipophilic dye-compatible brain clearing technique allowing correlative magnetic resonance/high-resolution fluorescence imaging in rat models of glioblastoma. Sci Rep. 2020; 10(1):1–15. Available from: https://doi.org/10.1038/s41598-020-75137-y PMID: 33087842

49. Moy AJ, Capulong B V., Saager RB, Wiersma MP, Lo PC, Durkin AJ, et al. Optical properties of mouse brain tissue after optical clearing with FocusClear™. J Biomed Opt. 2015 Sep 21; 20(9):095010. Available from: https://doi.org/10.1117/1.JBO.20.9.095010 PMID: 26388460

50. Moy AJ, Wiersma MP, Choi B. Optical Histology: A Method to Visualize Microvasculature in Thick Tissue Sections of Mouse Brain. PLoS One. 2013 Jan 23; 8(1):e53753. Available from: https://doi.org/10.1371/journal.pone.0053753 PMID: 23372668

51. Feng L, Zhao T, Kim J. neuTube 1.0: A New Design for Efficient Neuron Reconstruction Software Based on the SWC Format. eneuro. 2015 Jan 29; 2(1):ENEURO.0049-14.2014. Available from: https://doi.org/10.1523/ENEURO.0049-14.2014 PMID: 26464967

52. Dice LR. Measures of the Amount of Ecologic Association Between Species. Ecology. 1945; 26 (3):297–302.

53. Quintana DD, Lewis SE, Anantula Y, Garcia JA, Sarkar SN, Cavendish JZ, et al. NeuroImage The cerebral angiome: High resolution MicroCT imaging of the whole brain cerebrovasculature in female and male mice. Neuroimage. 2019; 202(April):116109. Available from: https://doi.org/10.1016/j.neuroimage.2019.116109 PMID: 31446129

54. Wälchli T, Bisschop J, Miettinen A, Ulmann-schuler A, Hintermüller C, Meyer EP, et al. Hierarchical imaging and computational analysis of three-dimensional vascular network architecture in the entire postnatal and adult mouse brain. Nat Protoc. 2021; 16(October). Available from: https://doi.org/10.1038/s41596-021-00587-1 PMID: 34480130

55. Hahn A, Bode J, Alexander A, Karimian-jazi K, Schregel K, Schwarz D, et al. Large-scale characterization of the microvascular geometry in development and disease by tissue clearing and quantitative ultramicroscopy. J Cereb Blood Flow Metab. 2021; 41(7):1536–46. Available from: https://doi.org/10.1177/0271678X20961854 PMID: 33043767

56. Berg S, Kutra D, Kroeger T, Straehle CN, Kausler BX, Haubold C, et al. ilastik: interactive machine learning for (bio) image analysis. Nat Methods. 2019; 16(December). Available from: https://doi.org/10.1038/s41592-019-0582-9 PMID: 31570887

57. Takahashi K, Abe K, Kubota SI, Fukatsu N, Morishita Y, Yoshimatsu Y, et al. An analysis modality for vascular structures combining tissue-clearing technology and topological data analysis. Nat Commun. 2022; 13(1):5239. Available from: https://doi.org/10.1038/s41467-022-32848-2 PMID: 36097010

58. Zhu J, Deng Y, Yu T, Liu X, Li D, Zhu D. Optimal combinations of fluorescent vessel labeling and tissue clearing methods for three-dimensional visualization of vasculature. Neurophotonics. 2022; 9(4). Available from: https://doi.org/10.1117/1.NPh.9.4.045008 PMID: 36466188

59. McDonald DM. Angiogenesis and Vascular Remodeling in Inflammation and Cancer: Biology and Architecture of the Vasculature. In: Angiogenesis. Boston, MA: Springer US; 2008. p. 17–33. Available from: https://doi.org/10.1007/978-0-387-71518-6_2

60. Li T, Kang G, Wang T, Huang H. Tumor angiogenesis and anti-angiogenic gene therapy for cancer (Review). Oncol Lett. 2018 May 17; 16(1):687–702. Available from: https://doi.org/10.3892/ol.2018.8733 PMID: 29963134

61. Datta A, Sarmah D, Mounica L, Kaur H, Kesharwani R, Verma G, et al. Cell Death Pathways in Ischemic Stroke and Targeted Pharmacotherapy. Transl Stroke Res. 2020 Dec 26; 11(6):1185–202. Available from: https://doi.org/10.1007/s12975-020-00806-z PMID: 32219729